

- bution to the change in surface area. The protein engineering experiments (10) used the truncated protein.
28. B. A. Schoemaker, J. Wang, P. G. Wolynes, *Proc. Natl. Acad. Sci. U.S.A.* **94**, 777 (1997).
  29. J. N. Onuchic, N. D. Socci, Z. Luthey-Schulten, P. G. Wolynes, *Folding Design* **1**, 441 (1996).
  30. Li and Daggett (16) focus on the value of  $\Phi_{MD}(t)$  at a selected transition state. We have monitored  $\Phi_{MD}(t)$  during the entire trajectory for some of the present simulations as well as those of Li and Daggett.
  31. A. Chakrabarty, T. Kortemme, R. L. Baldwin, *Protein Sci.* **3**, 843 (1994).
  32. A. R. Fersht, *Proc. Natl. Acad. Sci. U.S.A.* **92**, 10869 (1995).
  33. B. Nölting *et al.*, *ibid.* **94**, 826 (1997).
  34. There is a difference between the contact analysis from the simulations and the protein engineering ex-

- periments; for example, the protein engineering experiments deal only with the effect of side-chain mutations, whereas the contact analysis of the simulations is based on main-chain interactions for secondary structure and on side-chain interactions for tertiary structure (Fig. 1).
35. P. J. Kraulis, *J. Appl. Crystallog.* **24**, 946 (1991).

7 July 1997; accepted 30 October 1997

## Atomic and Macroscopic Reaction Rates of a Surface-Catalyzed Reaction

J. Winterlin,\* S. Völkening, T. V. W. Janssens, T. Zambelli, G. Ertl

The catalytic oxidation of carbon monoxide (CO) on a platinum (111) surface was studied by scanning tunneling microscopy. The adsorbed oxygen atoms and CO molecules were imaged with atomic resolution, and their reactions to carbon dioxide (CO<sub>2</sub>) were monitored as functions of time. The results allowed the formulation of a rate law that takes the distribution of the reactants in separate domains into account. From temperature-dependent measurements, the kinetic parameters were obtained. Their values agree well with data from macroscopic measurements. In this way, a kinetic description of a chemical reaction was achieved that is based solely on the statistics of the underlying atomic processes.

Chemical kinetics—that is, the determination of rate equations as functions of macroscopic parameters like temperature, pressure, and concentrations—constitutes one of the main sources of information about the mechanisms of chemical reactions. An analysis of the kinetics is, however, connected with a fundamental problem—mentioned also in basic physical chemistry textbooks—that a reaction mechanism, the sequence of elementary steps by which a product is formed, cannot be uniquely established by kinetic measurements, because overlooked intermediate steps or other complications can never be ruled out (1). The reverse procedure, the derivation of the kinetics from a microscopic mechanism, is unique, allowing one to disprove possible microscopic models. As a means for a positive proof of a mechanism, reverse analysis has not been an option so far simply because the atomic scale was difficult to access experimentally. Here we present results of a study in which this reverse approach has been successfully pursued for a heterogeneous chemical reaction, the oxidation of CO molecules on a single-crystal Pt(111) surface. By means of scanning tunneling microscopy (STM), we resolved the reactants, observed their statistical reactions as functions of time, and derived a quantitative rate equation. The kinetic parameters thus obtained agree surprisingly well

with those from previous macroscopic measurements.

In several previous STM studies, qualitative mechanistic effects in chemical surface reactions could be identified, including site-specific reactivities, the formation of islands of the reactants, and in particular, effects of structural rearrangements of the metal substrate (reconstructions) (2–4). However, to our knowledge there have been no studies to date in which quantitative rate laws could be extracted from the atomically resolved surface processes (5) so that possible influences on the macroscopic kinetics is still an open question.

The oxidation of CO on Pt(111) was chosen here because it is a well-studied, model-like catalytic reaction (6, 7) and is relatively simple; it also represents the basis for the catalytic removal of CO from exhaust gases by oxidation on Pt surfaces. The reaction does not involve reconstructions and has been demonstrated to follow the so-called Langmuir-Hinshelwood mechanism (8), which generally underlies heterogeneous catalysis and assumes that the product is formed by reaction between the adsorbed reactants. In the present case, the reaction comprises the dissociative adsorption of oxygen (9), the molecular adsorption of CO (10), and the combination of the two surface-adsorbed species to CO<sub>2</sub> (8); the CO<sub>2</sub> molecules are immediately released into the gas phase (7, 11). There are, however, indications that the actual mechanism involves more complex features than this simple scheme: From temperature-

programmed desorption studies (12), it was concluded that the reacting adsorbed O atoms and CO molecules are not randomly distributed, but that the reaction takes place at the perimeters of oxygen islands. That the reactants in a surface reaction might be localized in separate domains is, in fact, a long-discussed notion for catalytic reactions in general, and effects on the kinetics have been predicted by simulations (13).

Despite the detailed knowledge of many features of the CO and O reaction on Pt(111), it is characteristic—and this holds also for most complex chemical processes such as catalytic reactions—that no mechanistic model exists that is fully consistent with all features of the kinetics, as is reflected by, for example, the coverage dependence of all of the reaction “constants” involved in the CO<sub>2</sub> production rates (6, 7). Also, the reaction at island edges was disputed on the basis of isotope mixing studies (14), which concluded a homogeneous reaction probability. A recent study on this subject (15) produced the unexpected result that oxygen atoms in the interior of islands are more reactive than isolated atoms.

Our investigations were performed in an ultrahigh-vacuum chamber with the use of a variable-temperature STM, which, along with the cleaning of the Pt sample, was described previously (16). The experiments concentrated on the surface reaction step  $\text{CO}_{ad} + \text{O}_{ad} \rightarrow \text{CO}_2$  (ad, adsorbed). In order to monitor the progress of the reaction as a function of time, we cooled the Pt sample, reducing the reaction rate to fit the speed of the STM equipment. According to previous studies, the reaction starts well below room temperature (11, 12). Experiments were performed as “titration experiments,” by first covering the sample with submonolayers of oxygen atoms, which were then reacted off by exposure to constant CO pressures.

After preparation of the oxygen layer [Fig. 1, time ( $t$ ) = 0], the oxygen atoms, which are imaged as dark dots [this is an electronic effect that has been predicted theoretically (17)], formed small islands, in agreement with previous observations (16). The periodic structure within the islands corresponded to the known (2×2) structure of chemisorbed oxygen atoms on Pt(111)

Fritz-Haber-Institut der Max-Planck-Gesellschaft, Faradayweg 4-6, D-14195 Berlin, Germany.

\*To whom correspondence should be addressed.

(18). Despite the low temperatures, the oxygen layer displayed considerable thermal fluctuations [consistent with recent diffusion measurements (16)], which manifested themselves as atomic exchange processes at the island perimeters; the dark streaks on the bright empty areas between the islands represent hopping events of atoms (19).

Adsorption of CO on this surface initially led to a lower mobility of the oxygen atoms and a higher degree of order of the  $(2 \times 2)$  structure (Fig. 1,  $t = 90$  and 140 s). The oxygen layer was apparently compressed into larger islands, which was most likely caused by the repulsive interaction between the CO molecules on the bare parts and the oxygen atoms (8). The total size of the  $(2 \times 2)$  area was still unchanged at this time. The CO molecules that must have been present on the areas in between were not yet visible because of their large mobility. [The altered appearance of the  $(2 \times 2)$  structure as a hexagonal pattern of bright spots may indicate that CO molecules also adsorbed on sites between the oxygen atoms in the  $(2 \times 2)$  phase, as found spectroscopically (20).] After 290 s, the  $(2 \times 2)$  fraction of the surface had started to shrink, marking the progress of the reaction. Simultaneously, and more evidently after 600 s, an additional or-

dered, streaky structure became visible on the initially structureless areas. This pattern represents the known  $c(4 \times 2)$  CO structure (21), in which the CO molecules are closely packed and immobilized, thereby becoming resolved by STM. The  $c(4 \times 2)$  phase can exist in three rotational domains, two of which are visible in the lower half of the 600-s image (22); the upper one changed its orientation in the following image (700 s). At this stage (images at 600, 700, and 1100 s), the  $c(4 \times 2)$  areas continuously grew and the  $(2 \times 2)$  areas shrank, demonstrating the progress of the reaction; as mentioned,  $\text{CO}_2$  desorbs directly upon formation and was not detected. By 2020 s, the reaction was complete (23).

The STM thus resolved both reactants (the CO only for sufficiently high coverage) and allowed us to monitor the reaction. The reactants were not randomly distributed, but were localized in separate domains, and the reaction was not taking place randomly, but was restricted to the boundaries between the oxygen-containing  $(2 \times 2)$  and the  $c(4 \times 2)$  CO domains.

This qualitative conclusion is supported by a quantitative analysis of the STM data: The reaction rate was evaluated by determination of the  $(2 \times 2)$ -covered fraction of a given area as a function of time at constant

CO pressure (Fig. 2). If normalized to the length of the boundaries between CO and O domains (squares in Fig. 2), this rate was practically constant; the rate equation can therefore be expressed as  $-dn_{\text{O}}/dt = kL$ , where  $n_{\text{O}}$  is the number of O atoms and  $L$  is the length of the domain boundaries (24). Within the mean-field approximation, which assumes a random distribution of the reactants, the rate should be proportional to the product of the coverages  $\Theta$ , which was not the case, as follows from normalization with  $\Theta_{\text{O}} \cdot \Theta_{\text{CO}}$  (crosses in Fig. 2). This analysis therefore confirms conclusions from previous kinetic studies (12). The complete  $^{16}\text{O}/^{18}\text{O}$  isotope mixing in the product  $\text{CO}_2$ , from which, in contrast, a homogeneous reaction probability was concluded in another study (14), was based on the assumption of an immobile oxygen layer, whereas the  $t = 0$  frame (Fig. 1) demonstrates the mobility of O atoms at temperatures as low as 250 K. The isotope mixing is hence fully consistent with the present findings (25).

Making use of the variable-temperature capability of our STM setup, we attempted to obtain kinetic parameters for the process  $\text{CO}_{\text{ad}} + \text{O}_{\text{ad}} \rightarrow \text{CO}_2$  by recording and analyzing data as for Fig. 2 over a (limited) temperature range in which no qualitative differences had been found. The resulting

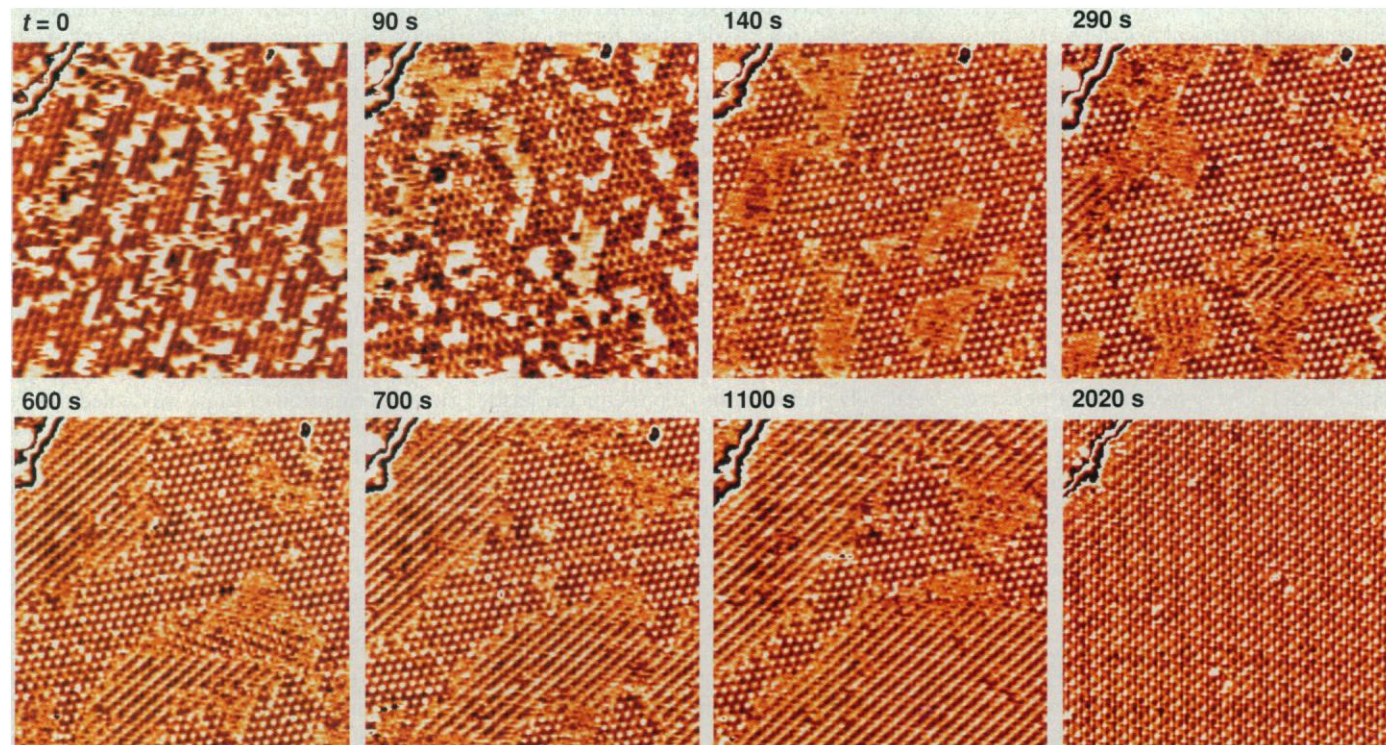


**Fig. 1.** Series of STM images, recorded during reaction of adsorbed oxygen atoms with co-adsorbed CO molecules at 247 K, all from the same area of a Pt(111) crystal. Before the experiment, a submonolayer of oxygen atoms was prepared (by an exposure of 3 Langmuirs  $\text{O}_2$  at 96 K, a short annealing to 298 K, and cooling to 247 K), and CO was continuously supplied from the gas phase ( $P_{\text{CO}} = 5 \times 10^{-8}$  mbar). At this pressure, the

impingement rate of CO molecules is about 1 monolayer per 100 s, where the zero-coverage sticking coefficient on the empty and oxygen-covered surface is about 0.7 (8); the times refer to the start of the CO exposure. The structure at the upper left corner is an atomic step of the Pt surface. Image sizes,  $180 \text{ \AA}$  by  $170 \text{ \AA}$ ; tunneling voltage (with respect to the sample), +0.5 V; tunneling current, 0.8 nA.

REFERENCES AND NOTES

Arrhenius plot (Fig. 3) yields an activation energy  $E^*$  of 0.49 eV and a preexponential factor of  $3 \times 10^{21}$  particles  $\text{cm}^{-2} \text{s}^{-1}$ . These microscopically determined kinetic parameters can be compared with existing data from macroscopic measurements. The activation energy for  $\text{CO}_2$  formation upon exposure of an O-saturated Pt(111) surface to a molecular beam of CO was derived to be  $E^* = 0.51$  eV (8), in excellent agreement with the present finding. [Even the value of 0.7 eV derived from temperature-programmed desorption experiments for similar conditions (12) is still in reasonable agreement, keeping in mind the limited reliabil-

ity of data from nonisothermal experiments.] The preexponential factor, reported in the quoted molecular beam study (8), was evaluated on the assumption of a mean-field rate equation; hence, the resulting quantity is not directly comparable with the one derived here (also, the units are different). It can be converted, however, into an equivalent quantity by assuming average O and CO concentrations of about  $10^{14}$  to  $10^{15}$  particles  $\text{cm}^{-2}$  each. This calculation leads to values of the order of  $10^{22}$  to  $10^{24}$  particles  $\text{cm}^{-2} \text{s}^{-1}$  for the preexponential factor, which is again in satisfactory agreement with the microscopic result. That the mean-field approximation could be applied in (8), although not giving the correct coverage dependence, is due to the fact that the high-coverage data points entering the analysis were each measured at equal coverages, at which the boundary lengths must have been about equal (26).

That the microscopically derived kinetic parameters and those from "classic" macroscopic rates are almost identical is, in fact, striking. Of course, agreement is to be expected when the correct atomic mechanism has been established, which, in this case, has been shown to require the knowledge of the spatial distribution of the reacting particles. For the oxidation of CO, there had been several indications that it is not correctly described by a uniform reaction probability: These signs include findings by electron diffraction that adsorbates during the reaction were localized in separate domains (27), and kinetic measurements showing a square root dependence on the coverage (28). However, as mentioned in the beginning, the kinetics alone cannot unambiguously prove a mechanism. Nevertheless, macroscopic rates are often interpreted in terms of atomic models, which is not unique, as is illustrated by the contrasting interpretation of previous (macroscopic) experiments on the present, relatively simple reaction (12, 14, 15). In more complicated cases, there is usually so little information about the mechanism that the kinetics serves only as a phenomenological method for a quantitative description of reaction rates, often containing coverage-dependent reaction constants, and the modeling of industrial catalytic processes ["microkinetic analysis" (29)] is still based on the mean-field approximation. Predictions about rates from microscopic mechanisms that are more complex than the mean-field approximation have been restricted so far to simulations, mostly by Monte Carlo methods [for example, (13)]. The present work quantitatively verifies the macroscopic kinetics for a chemical reaction on the basis of experimental information on the atomic scale.

1. K. J. Laidler, *Chemical Kinetics* (Harper & Row, New York, 1987).
2. L. Ruan, F. Besenbacher, I. Stensgaard, E. Lægsgaard, *Phys. Rev. Lett.* **69**, 3523 (1992); F. M. Leibsle, P. W. Murray, S. M. Francis, G. Thornton, M. Bowker, *Nature* **363**, 706 (1993); F. M. Leibsle *et al.*, *Phys. Rev. Lett.* **72**, 2569 (1994); W. W. Crew and R. J. Madix, *Surf. Sci.* **319**, L34 (1994); P. T. Sprunger, Y. Okawa, F. Besenbacher, I. Stensgaard, K. Tanaka, *ibid.* **344**, 98 (1995).
3. W. W. Crew and R. J. Madix, *Surf. Sci.* **349**, 275 (1996).
4. T. Zambelli, J. Winterlin, J. Trost, G. Ertl, *Science* **273**, 1688 (1996).
5. In one study about CO oxidation on Cu(110) (3), a kinetic analysis was performed, but the authors had to assume a reaction model (basically a mean-field approximation) because at 400 K, the CO molecules and the reactive O species were not resolved. Also, no temperature variation was performed.
6. T. Engel and G. Ertl, in *Advances in Catalysis*, D. D. Eley, H. Pines, P. Weisz, Eds. (Academic Press, New York, 1979), vol. 28, pp. 1-78.
7. ———, in *The Chemical Physics of Solid Surfaces and Heterogeneous Catalysis*, D. A. King and J. P. Woodruff, Eds. (Elsevier, Amsterdam, 1982), vol. 4, pp. 73-93.
8. C. T. Campbell, G. Ertl, H. Kuipers, J. Segner, *J. Chem. Phys.* **73**, 5862 (1980).
9. N. R. Avery, *Chem. Phys. Lett.* **96**, 371 (1983).
10. H. Froitzheim, H. Hopster, H. Ibach, S. Lehwald, *Appl. Phys.* **13**, 147 (1977).
11. K.-H. Allers, H. Pfnür, P. Feulner, D. Menzel, *J. Chem. Phys.* **100**, 3985 (1994).
12. J. L. Gland and E. B. Kollin, *ibid.* **78**, 963 (1983).
13. M. Silverberg, A. Ben-Shaul, F. Rebenrost, *ibid.* **83**, 6501 (1985).
14. S. Akhter and J. M. White, *Surf. Sci.* **171**, 527 (1986).
15. M. Xu, J. Liu, F. Zaera, *J. Chem. Phys.* **104**, 8825 (1996).
16. J. Winterlin, R. Schuster, G. Ertl, *Phys. Rev. Lett.* **77**, 123 (1996).
17. N. D. Lang, *Comments Condens. Matter Phys.* **14**, 253 (1989).
18. J. L. Gland, B. A. Sexton, G. B. Fisher, *Surf. Sci.* **95**, 587 (1980).
19. The dynamics of the system is similar to that of O atoms on Ru(0001) at 300 K, where the fluctuations could be followed in real time (J. Winterlin *et al.*, *Surf. Sci.*, in press).
20. J. L. Gland and E. B. Kollin, *Surf. Sci.* **151**, 260 (1985).
21. G. Ertl, M. Neumann, K. M. Streit, *ibid.* **64**, 393 (1977).
22. That they appear to display different atomic structures is an imaging artifact caused by an asymmetric tip.
23. The somewhat different appearance of the  $c(4 \times 2)$  CO phase in this panel is the result of an intermediate change in imaging conditions of the tunneling tip.
24. The slight increase of the normalized rate was caused by the fact that in the course of the reaction, not only the length but also the shape of the boundary and thereby the average coordination of the oxygen atoms at the  $(2 \times 2)$  perimeters changed. This effect can be included in a more precise description of the kinetics by Monte Carlo simulations, which we have also performed. In the present context, the rate increase can be neglected.
25. However, for the finding in the third study (15)—that differently prepared oxygen layers (with the same coverages) display different reactivities at 350 K—we do not have an explanation so far. After heating to 600 K and cooling to 350 K, when the effect was observed in the quoted paper, the oxygen distribution is in equilibrium, according to our data, and should be independent of the preparation.
26. At higher temperatures, or equivalently under low-coverage conditions, both cited kinetic studies (8, 12) reveal much larger activation energies (1.05 and 1.7 eV, respectively), indicating a different reaction mechanism. At low coverages, the adsorbates exhibit larger adsorption energies, so

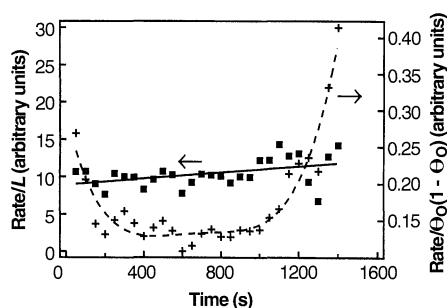


**Fig. 2.** Reaction rates, determined from the change of the size of the  $(2 \times 2)$  area between successive panels of the data of Fig. 1 (the series actually contains more and larger images than those shown in Fig. 1), normalized to (squares) the length of the boundary between oxygen and CO domains (the full line is a linear fit) and (crosses) divided by  $\Theta_O(1 - \Theta_{CO})$ , which is equal to  $\Theta_O \cdot \Theta_{CO}$  if  $\Theta = 1$  implies maximum coverage of the respective phase (the broken line is only to guide the eye).

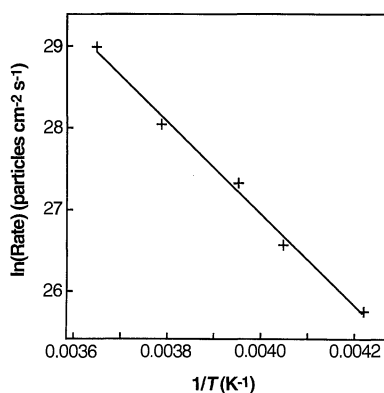


**Fig. 3.** Arrhenius plot of reaction rates between 237 and 274 K (temperature range limited by the recording speed of the STM), determined by evaluating the changes in the number of oxygen atoms within given areas at fixed, intermediate lengths of the domain boundaries. The CO pressure ensured that even at the highest rates, the supply of CO molecules from the gas phase was not limiting, as confirmed by the observation of the  $c(4 \times 2)$  CO structure over the whole temperature range, indicating high coverage conditions, and by the fact that the rate was independent of the CO pressure between  $5 \times 10^{-8}$  and  $5 \times 10^{-7}$  mbar.

- that an increase of the activation energy becomes plausible.
27. H. Conrad, G. Ertl, J. Küppers, *Surf. Sci.* **76**, 323 (1978).
28. M. A. Barteau, E. I. Ko, R. J. Madix, *ibid.* **104**, 161 (1981).

29. J. A. Dumesic, D. F. Rudd, L. M. Aparicia, J. E. Rekoske, A. A. Trivino, *The Microkinetics of Heterogeneous Catalysis* (American Chemical Society, Washington, DC, 1993).

18 August 1997; accepted 30 October 1997

## Growth of SiO<sub>2</sub> at Room Temperature with the Use of Catalyzed Sequential Half-Reactions

Jason W. Klaus, Ofer Sneh,\* Steven M. George†

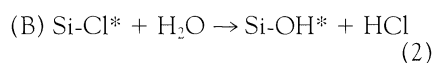
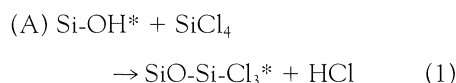
Films of silicon dioxide (SiO<sub>2</sub>) were deposited at room temperature by means of catalyzed binary reaction sequence chemistry. The binary reaction SiCl<sub>4</sub> + 2H<sub>2</sub>O → SiO<sub>2</sub> + 4HCl was separated into SiCl<sub>4</sub> and H<sub>2</sub>O half-reactions, and the half-reactions were then performed in an ABAB . . . sequence and catalyzed with pyridine. The pyridine catalyst lowered the deposition temperature from >600 to 300 kelvin and reduced the reactant flux required for complete reactions from ~10<sup>9</sup> to ~10<sup>4</sup> Langmuirs. Growth rates of ~2.1 angstroms per AB reaction cycle were obtained at room temperature for reactant pressures of 15 millitorr and 60-second exposure times with 200 millitorr of pyridine. This catalytic technique may be general and should facilitate the chemical vapor deposition of other oxide and nitride materials.

The reduction of thin films to nanometer dimensions for new technologies requires exquisite control of film thickness, morphology, crystallinity, and conformality (1). Lower deposition temperatures are also required because interlayer diffusion may destroy the properties of nanoscale devices. Many of these requirements can be achieved by growth controlled at single atomic layers by means of binary reaction sequence chemistry (2).

SiO<sub>2</sub> is the optimal dielectric material in silicon microelectronic devices. Conformal SiO<sub>2</sub> film deposition on trench capacitors with high aspect ratios will be needed as interface layers to extend dynamic random access memory (DRAM) to the 1-gigabyte regime (3). Future flat panel displays will require uniform and precise SiO<sub>2</sub> film deposition on extremely large substrates (4). In addition, very thin SiO<sub>2</sub> films can be used in multilayer and nanolaminate structures to tailor mechanical, electrical, and optical thin film properties (5). Low-temperature SiO<sub>2</sub> deposition techniques will also facilitate the use of SiO<sub>2</sub> as a protective coating or insulator on polymeric or biological materials.

Self-terminating surface reactions applied in a binary reaction sequence can be used to achieve atomic layer control of thin film growth (2, 6–9). Recent work on SiO<sub>2</sub> atomic layer-controlled growth has focused

on dividing the SiCl<sub>4</sub> + 2H<sub>2</sub>O → SiO<sub>2</sub> + 4HCl reaction into two half-reactions (6):



where the asterisks designate the surface species. The SiCl<sub>4</sub> and H<sub>2</sub>O half-reactions are performed in an ABAB . . . binary sequence to grow SiO<sub>2</sub>.

In each half-reaction, a gas-phase precursor reacts with a surface functional group. The surface reaction continues until all of the initial surface functional groups have reacted and have been replaced with the new functional group. Successive application of the A and B half-reactions has produced atomic layer-controlled SiO<sub>2</sub> deposition (9). Atomic force microscope (AFM) images revealed that the SiO<sub>2</sub> films deposited on Si(100) were highly conformal and extremely smooth (9). The only drawback was the high temperatures (>600 K) and large reactant exposures [ $>10^9$  Langmuirs (1 L = 10<sup>-6</sup> torr s)] required for the surface half-reactions to reach completion.

We now show that high reaction temperatures and large precursor fluxes can be avoided by catalyzing the surface reactions. We chose the organic base pyridine (C<sub>5</sub>H<sub>5</sub>N) as the catalyst because pyridine interacts strongly with the surface functional groups and reactants present during both the SiCl<sub>4</sub> and H<sub>2</sub>O half-reactions of the binary reaction sequence (10). Pyridine is also a very stable molecule, and this stability minimized incorporation of N or C into

the deposited SiO<sub>2</sub> film.

We observed no uncatalyzed SiO<sub>2</sub> film growth on our Si(100) wafer at 300 K after five AB cycles for reactant exposures as large as 10<sup>10</sup> L during the A and B half-reactions (11). In contrast, the addition of a small amount of pyridine initiated immediate SiO<sub>2</sub> film growth. The effect of pyridine was quantified by measuring SiO<sub>2</sub> film deposition as a function of pyridine partial pressure using fixed reactant exposures of 15 mtorr for 15 s. Pyridine accelerated the half-reactions with increasing pyridine partial pressures up to 2.0 torr. Pressures greater than 2.0 torr resulted in no further measurable enhancement of the reaction efficiency.

The dependence of the half-reactions on the A and B reactant exposure time (reactant pressure, 15 mtorr) was examined by measuring the SiO<sub>2</sub> film thickness deposited by five AB cycles at 290 K (Fig. 1). The pyridine partial pressure was fixed at 200 mtorr to allow shorter pumping times between the reaction cycles. The SiCl<sub>4</sub> exposure times were equal to the H<sub>2</sub>O exposure times. A typical AB cycle occurred with the following sequence: Expose pyridine (200 mtorr); dose SiCl<sub>4</sub> (15 mtorr) for variable reaction times; evacuate (10<sup>-4</sup> torr); expose pyridine (200 mtorr); dose H<sub>2</sub>O (15 mtorr) for variable reaction times; evacuate (10<sup>-4</sup> torr).

The half-reactions are self-limiting; once a half-reaction goes to completion, additional reactant produces no additional film growth. To determine which half-reaction is slower, we studied the SiO<sub>2</sub> film growth versus H<sub>2</sub>O exposure time with a fixed SiCl<sub>4</sub> exposure time. The SiCl<sub>4</sub> and H<sub>2</sub>O pressures were equal. The SiO<sub>2</sub> growth rate did not decrease until the H<sub>2</sub>O exposure time was one-fourth that of the SiCl<sub>4</sub> exposure time, which indicates that the SiCl<sub>4</sub>

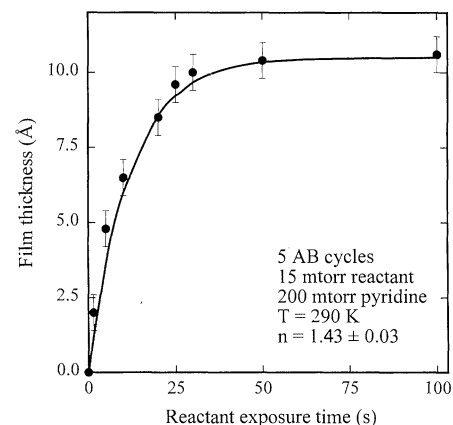


Fig. 1. Ellipsometric measurements of SiO<sub>2</sub> film thickness deposited by five AB cycles at 290 K for various reactant exposure times at reactant pressures of 15 mtorr with 200 mtorr of pyridine.

Department of Chemistry and Biochemistry, University of Colorado, Boulder, CO 80309, USA.

\*Present address: Lucent Technologies–Bell Laboratories, Optoelectronics Center, Breinigsville, PA 18031, USA.

†To whom correspondence should be addressed.